Food Sci. Technol. Res., **14** (1), 74–82, 2008

Technical paper

A Dedicated MRI for Food Science and Agriculture

Mika KOIZUMI[1], Shigehiro NAITO[1], Nobuaki ISHIDA[1*], Tomoyuki HAISHI[2] and Hiromi KANO[3]

[1] *National Food Research Institute, Tsukuba, Ibaraki 305-8642, Japan*

[2] *MRTechnology, Inc., Tsukuba, Ibaraki 305-8573, Japan*

[3] *Oak-Hill Georgic Patch-Work Laboratory, 4-13-10 Miyamoto, Funabashi, Chiba 273-0003, Japan*

Received October 10, 2006; Accepted August 27, 2007

A dedicated magnetic resonance imaging (MRI) apparatus that is small, lightweight, and usable in an ordinary research room was devised for developmental research and quality estimation of foods and agricultural products. The thawing processes of frozen margarine and meats were traced, the distributions of oils in adipose tissue (fat) and water in muscle tissue for pork and beef were distinctively visualised, the oil-accumulating tissues in seeds and the sticky materials on surface of fermented soybeans (*natto*) were characterised, and the three-dimensional organisation of the fine vasculature in fruits was visualised by the apparatus. The proton-specified MRI was easy to operate and provided well depicted images of internal structures, the distribution and mobility of water and oils, and susceptibility differences inside materials, demonstrating that the devised machine is useful for food and agricultural research.

Keywords: small dedicated magnetic resonance imaging (MRI), proton-specified apparatus, frozen margarine, frozen meats, *natto*, fruits

Introduction

Magnetic resonance imaging (MRI) non-destructively provides information on internal conditions for gross materials (McCarthy, 1994; Faust *et al.*, 1997; Hills, 1998), and has been effectively used in food science and agricultural research. Unfortunately, however, it is not widely used because the machine is large, expensive, and difficult to operate.

Small MRI apparatuses have been developed from the late 1990s for use in research rooms adjacent to material production sites. However, the image quality was unstable, and the apparatuses were usually specialised for specific objectives. These issues result from the low field permanent magnets used for the apparatuses. The field strength of permanent magnets is strongly affected by the ambient temperature (Haishi *et al.*, 2001), and the inhomogeneity in a low magnetic field is difficult to regulate in the construction of the magnet (Constantinesco *et al.*, 1997). In the present brief paper, we report a small, dedicated MRI apparatus devised and improved for use in developmental research and quality estimation of foods and agricultural products.

*To whom correspondence should be addressed.
E-mail: nobu@affrc.go.jp

The apparatus was constructed based on the system previously reported by Haishi *et al.* (2001), which was a small proton MRI spectrometer (MRTechnology Inc., Tsukuba, Japan) equipped with a 1.0 Tesla (T: unit indicating the magnitude of a magnet) permanent magnet with a 60-mm pole gap (Neomax Co., Ltd., Saga, Japan) and a solenoid detector with gradient circuits for imaging. The following were introduced to overcome the defects associated with common small MRI apparatuses and to make the apparatus usable for various materials employed in foods and agricultural products. The magnetic field used was stronger than a similar small MRI system using a 0.2 T permanent magnet (Constantinesco *et al.*, 1997). A stronger magnetic field was advantageous for detecting weak signals and for obtaining good quality images with an adequate spatial resolution. During the current development of the small MRI, Neomax Co., Ltd. provided a newly devised temperature stabiliser for suppressing drifts in the magnetic field strength of the permanent magnet due to fluctuations in the ambient temperature. The offset current supplied for the gradient circuits in the detector was used as an effective shim system for minimising inhomogeneity in the magnetic field. Such improvements in accessories for imaging enabled us to configure a small, lightweight, and easily

operable MRI that can be placed in an ordinary, lightly air-conditioned research room.

Typical examples of food material measurements by the apparatus are presented. The thawing of frozen margarine and meats was examined, the distribution and mobility of water and oils were determined for meats and fermented soybeans (*natto*), and the internal structures of fruits were depicted using the apparatus. The usefulness of the apparatus in food science and agricultural research is discussed based on the results.

Materials and Methods

Figure 1 illustrates the apparatus that is composed of a small permanent magnet of 60 × 40 cm^2 and 40 cm high with a 60-mm pole gap (approximately 300 kg in weight) (Neomax Co. Ltd.) (A), an MRI spectrometer with dimensions of 60 cm square and 80 cm high (approximately 100 kg in weight) (B), and a console display consisting of liquid-crystal screen with a keyboard (C). A detachable, high-frequency sweeper for adjusting the resonating frequency is used to operate the apparatus. The apparatus is located in a lightly air-conditioned research room kept at 25°C.

The operating system was built on a personal computer using Microsoft Windows 98 (Microsoft Japan, Tokyo, Japan). A new or a modified pulse sequence for measurements was written as a text file and compiled. Floating point (4 byte, Windows) image data were acquired and Fourier transformed to 16 bit-unsigned, little endian byte order format for display. The temperature of the magnet was kept at 28°C by a specially designed temperature stabiliser. The measurement cell was maintained at the same temperature. A 30-mm diameter gradient probe was created. The field of view (FOV) was set at the maximum volume, a 30-mm cube (gradient magnetic field strengths: Gx=40 mT/m; Gy=35 mT/m; and Gz=52 mT/m), for observing food materials.

A sample was inserted into a hole with the gradient circuits and the detector coil between the pole pieces of the magnet (Fig. 1D) using a disposable plastic test tube of 30 mm in diameter as a sample holder (Fig. 1E). The resonance frequency was adjusted for protons (42.6 MHz), and the resonance condition of the detector coil was matched for imaging. The signal shape was then improved by supplying offset currents for the gradient circuits in the detector as the acquired spectral peak was single and symmetric. After the imaging parameters were set, the measurements were started by the spin-echo 2D Fourier Transform (FT) method, the spin-echo 3D-FT method or the gradient-echo 3D-FT method. The repetition time (TR) was 0.1, 0.2 or 1 s, and the echo time (TE), 2.2, 7 or 40 ms. Data points of 128 or 256, 128 encoded steps, and a slice thickness of 1.8 or 3.6 mm were employed to obtain adequate signal intensity for two-dimensional measurements. Images were created on a matrix of 128 × 128 or 256 × 256 with a 234 or 117 μm planar resolution and a 1.8 or 3.6 mm slice thickness. One hundred and twenty-eight slice images with a 234-μm inter-slice distance were obtained for three-dimensional measurements, and images were created on a 128 × 128 × 128 matrix with a 234-μm spatial resolution. The conditions for each measurement are listed in Table 1.

Data were processed and images were created by using Scion Image program [Public domain NIH Image program (National Institutes of Health, Bethesda, MD, USA) translated for Windows operating systems by Scion Co., Frederick, MD, USA; available on the Internet at http://www.scioncorp.com], ImageJ [a public domain Java image processing program (ver. 1.33); available on the Internet at http://rsb.info.

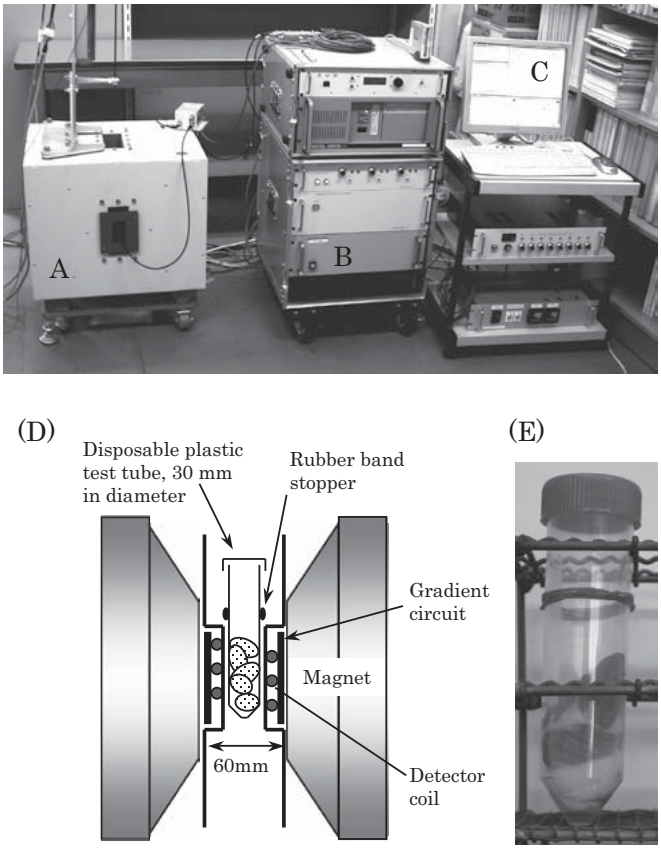

Fig. 1. Small MRI for food and agricultural research. (A) Permanent magnet with 1.0 T of field strength, 60 × 40 cm^2 and 40 cm high. (B) Spectrometer of 60 × 60 cm^2 and 80 cm high with a computer system. (C) Console display consisting of the liquid-crystal screen with a keyboard. There is a shim controller for fine shimming and minimising inhomogeneity of the magnetic field under the display and the keyboard. (D) The block diagram around the measurement cell. The pole gap of the magnet is 60 mm. There are circuits for generating gradient magnetic fields and a detection coil inside them. (E) Materials were placed in a plastic disposable test tube 30 mm in diameter as a holder.

Table 1. Materials and measuring conditions.

Figure	Materials	Method	TR (s)	TE (ms)	Acquisition	Measuring time	Pixel size or voxel size (μm)	Slice thickness (mm)	Section
2	Frozen margarine (-40°C)	2D spin-echo	0.2	7	4	103 sec/image	117 (256×256) [a]	1.8	horizontal
3	Thawed pork	3D gradient-echo	0.2	2.2	1	55 min/ image set	234 (128×128×128)		vertical
4	Frozen pork (-20°C)	2D spin-echo	1	7	1	128 sec/image	234 (128×128)	3.6	vertical
5	Frozen beef (-20°C)	2D spin-echo	1	7	1	128 sec/image	234 (128×128)	3.6	vertical
6A	Frozen pork (-20°C)	NMR spectra							
6B	Frozen beef (-20°C)	(FID signal)							
7A	Fermented soybean	3D spin-echo	0.1	7	4	112 min/image set	234		horiz&vert
7B	(*natto*) before stirring	3D spin-echo	1	40	4	1092 min/image set	234 (128×128×128)		horiz&vert
8A	Fermented soybean	3D spin-echo	0.1	7	4	112 min/image set	234		horiz&vert
8B	(*natto*) after stirring	3D spin-echo	1	40	4	1092 min/ image set	234 (128×128×128)		horiz&vert
9	Sweet cherry (*Prunus avium* L.)	3D spin-echo	0.2	7	2	109 min/ image set	234 (128×128×128)		vertical
10	Blueberry (*Vaccinium ashei*)	3D spin-echo	0.2	7	2	109 min/ image set	234 (128×128×128)		vertical

[a]Numbers in parentheses indicate the image matrix.

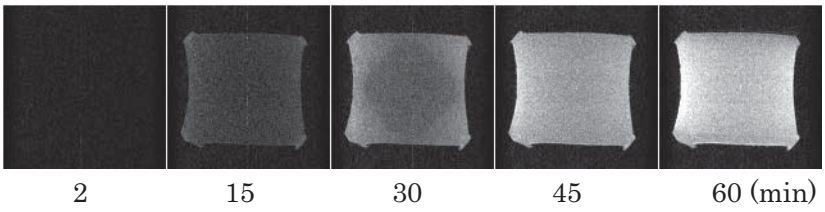

Fig. 2. Changes in frozen margarine images during thawing. A horizontal section was measured by the spin-echo 2D-FT method with TR of 0.2 s and TE of 7 ms. Images were acquired at 2 min and continuously with 5-min intervals after 5 min. Images at 2, 15, 30, 45 and 60 min are presented. No signal was detected at 2 min. The dark area (late thawing area) was observed at 30 min.

nih.gov/ij/], and NMRv2b [rendering software (MRTechnology Inc.)].

Materials were obtained from markets. Margarine was frozen to induce changes in physical properties in the material. Other materials included pork and beef samples of frozen foods, fermented soybeans (*Glycine max*), *natto*, a fermented food, and sweet cherries (*Prunus avium* L.) and blueberries (*Vaccinium ashei* Reade) to be eaten uncooked.

Results and Discussion

Imaging of transient heat transfer in frozen margarine

MRI does not yield signals for frozen materials where all compounds have lost mobility, but does yield a signal after the materials thaw and compounds acquire mobility. Therefore, the freezing and thawing processes of materials can be traced (Brennan *et al.*, 1997; Kerr *et al.*, 1998; Price *et al.*, 1997). Thawed compounds increase their mobility with increasing temperature, which intensifies image signals.

Figure 2 illustrates thawing of frozen margarine. Margarine was frozen at -40°C and time-lapse images in a horizontal section were then measured at 2 min and at 5-min intervals after 5 min of natural thawing at 28°C. The frozen material is dark at 2 min, and an image appears at 15 min, which is primarily due to the signal of mobile oils contained between oil crystals. The signal develops with time, and the transient thaw area is observed around a diagonal square of the darker area of the image at 30 min. Heat conduction was not isotropic; heat transferred faster through the corners touching the wall of the test tube than through the side sections because the air space between the wall of the test tube and the material more severely restricted the rate of heat transfer. The signal covers all areas of the margarine at 45 min, and intensity strongly increases thereafter, partly due to increasing amounts of mobile oil molecules and partly due

to the increasing mobility of the molecules with the elevation of temperature in the material. Similar phenomena were also reported for frozen vegetables. The signal appeared and increased in intensity with time, while the area of remaining ice decreased. The transient heat transfer and kinetics of the thawing process were visualised and analysed using the images (Koizumi *et al.*, 2006a). Freezing processes may also be analysed in a similar way using MRI (Kerr *et al.*, 1998; Hills, 1998).

Distinguishing fat and muscle tissues of meats and their quantitative characteristics MRI can distinctively image the fat and muscle tissues of a piece of meat (McCarthy, 1994; Laurent *et al.*, 2000; Renou *et al.*, 2003). Moreover, the morphological, textural, and physical changes before freezing and after thawing were detectable (Guiheneuf *et al.*, 1997; Hall *et al.*, 1998). The distribution of the fat or adipose tissue and the muscle tissue in thawed pork was measured by the 3D gradient-echo method. The images clearly depicted the fat and muscle tissues in the meat at freely selected slice positions (Fig. 3A). Oil signals in the fat tissue were emphasised in the images using a short TR of 0.2 s due to the saturation of the spin excitation in water with long spin-lattice relaxation times (T_1), i. e., T_1-weighted images. The volume rendering image (Fig. 3B) could depict the spatial distribution of the fat tissue in the meat using a set of three-dimensional measurements. Rotation of the volume rendering image was helpful for understanding the detailed location of the fat tissue in the meat sample.

The frozen pork and beef stored at -20°C were naturally thawed in the measurement cell at 28°C. Time-lapse images in vertical sections and NMR spectra were simultaneously obtained at 5-min intervals. Figure 4 presents images of thawing pork acquired by the spin-echo 2D-FT method with a long TR of 1 s. The MRI images obtained with the long TR

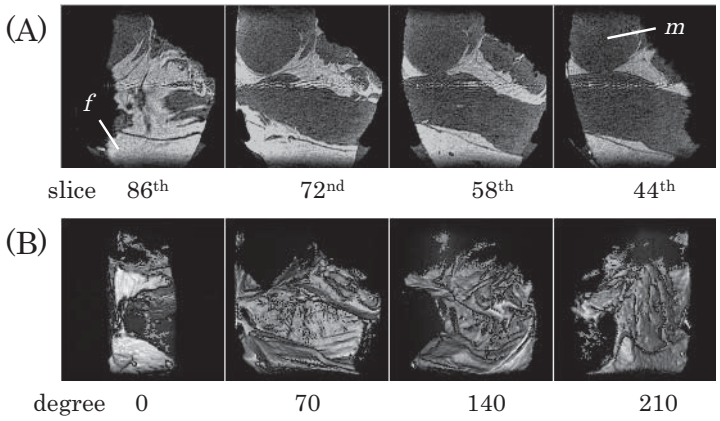

Fig. 3. Distribution of muscle and fat tissues in a piece of pork. The measurement was carried out using thawed pork by the gradient-echo 3D-FT method with TR of 0.2 s and TE of 2.2 ms. (A) Digitally sliced section from a set of three-dimensional image data. Vertical sections of 86th, 72nd, 58th and 44th of 128 slices are presented. *m* indicates muscle tissue and *f*, fat tissue. (B) Volume rendering expression of the three-dimensional image data indicating the distribution of the fat tissue. Rotated images at 0, 70, 140 and 210 degrees are presented.

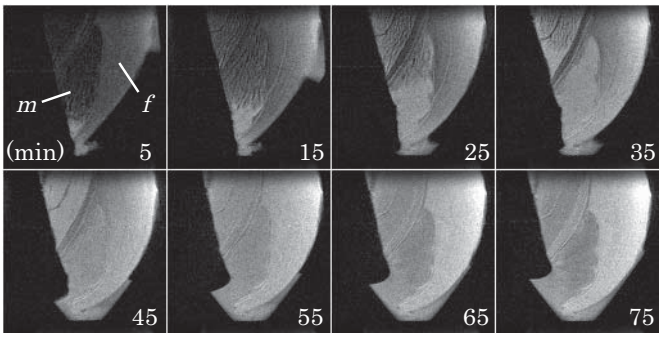

Fig. 4. Changes in frozen pork images during thawing. A vertical section was measured. TR was set to 1 s, and TE, to 7 ms. Signals came from both water and oils. Images acquired continuously with 5-min intervals and those at 5, 15, 25, 35, 45, 55, 65 and 75 min are presented. The signal of fat tissue (right side, *f*) increased first, then water in muscle tissue (left side, *m*) was thawed from the part attached to the bottom of the test tube (Fig. 1E).

detect water in the muscle tissue as well as oils in the fat tissue for the meat. Weak signals were observed in the area of the fat tissue at the start of acquisition. The oil signal in the fat tissue intensified first. The water signal in the muscle tissue then spread from the bottom of the test tube until the material was covered with the signals at 45 min. The signals in the fat tissue then intensified again in the last stages of thawing. Similar images were obtained for beef (Fig. 5), as water signals initially intensified in the muscle tissue up until 50 min. The signals of fat tissue then increased during thawing and finally exceeded the intensity of the muscle signals. TR was set at 1 s from the results of preliminary measurements in order to obtain clear time-separated images indicating the phase transition from solid to liquid by minimizing the time required for an image. However, in contrast, a slight suppression of the water signal contrasting the fat tissue was seen in the muscle tissue after being fully thawed (Figs. 4 and 5). This might be due to the saturation of spin excitation with the elevation of temperature and the elongation in T_1 of water molecules.

The NMR spectra of the materials could supply additional information about the individual properties of oils and water between the two meats (Fig. 6). The right peak near 1 ppm in the spectra indicates oils, and the left peak around 5 ppm indicates water (Beauvallet and Renou, 1992). Oils were not completely frozen in the pork at 0 min, and some oil was thought to remain mobile during low-temperature storage at -20°C (Fig. 6A). In contrast, more water was mo-

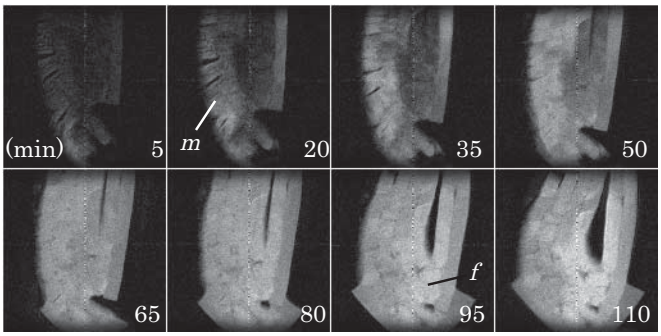

Fig. 5. Changes in frozen beef images during thawing. A vertical section was measured. TR was set to 1 s, and TE, to 7 ms. Signals came from both water and oils. Images acquired continuously with 5-min intervals and those at 5, 20, 35, 50, 65, 80, 95 and 110 min are presented. The water signals of muscle tissue (left side, *m*) increased first, then the signal of fat tissue (right side, *f*) intensified. The shape of the sample deformed after 80 min, which indicates that ice had been thawed and the integrity of the sample was lowered.

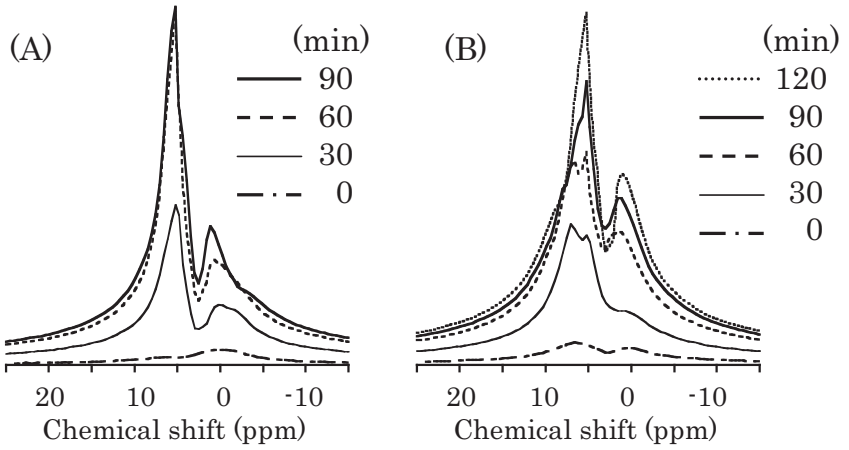

Fig. 6. Changes in NMR spectra of frozen pork and beef during thawing. The NMR spectra of the pork (A) and the beef (B) used in the measurements of Figs. 4 and 5 are shown. The numbers on lines on the right above the NMR spectra indicate times after the start of thawing. A free induction decay (FID) signal was acquired at individual times and Fourier transformed. Most water signals and oil signals were detected. The peaks near 1 ppm (right peak) in the spectra are those of oils, and those around 5 ppm (left peak) are of water. An oil signal was observed at 0 min from the start of thawing for pork (A), while the water signal was larger than that of oils for beef (B). A considerable part of the oil thawed before 30 min for pork (A) and most of the oil after 30 min for beef (B).

bile than oils at 0 min in the frozen beef, and the water peak rapidly intensified prior to oils after the initiation of thawing (Fig. 6B). Comparing the spectral changes in water and oils around 30 min between the pork (Fig. 6A) and the beef (Fig. 6B), the beef fat thawed more slowly than the pork fat.

Internal structure and sticky materials of natto Structural or architectural information is obtained using relaxation-time weighted images and three-dimensional images (Chudek and Hunter, 1997). Fermented soybean, *natto*, a traditional Japanese food, was measured by emphasising signals of the internal structures and oils concentration areas using a short TR in relation to T_1 (Figs. 7A and 8A) and by emphasising the sticky materials using a long TE in relation to spin-spin relaxation time (T_2) (Figs. 7B and 8B) with the spin-echo method (Koizumi *et al.*, 2006b). The former intensifies the signals of the compound with low mobility, such as water restricted in motion by interactions with solid structures and large oils molecules. The latter intensifies the signals of the compounds with high mobility, such as free water molecules in the sticky materials. Soybeans fully soaked overnight

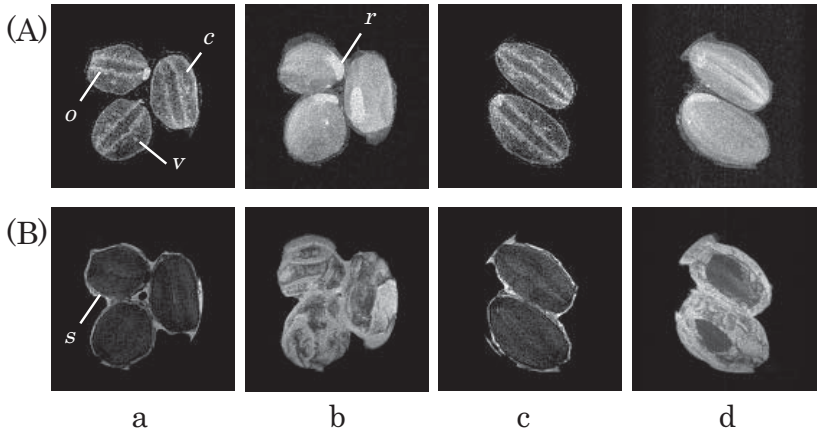

Fig. 7. Three-dimensional measurement of fermented soybeans, *natto*, before stirring. The images were acquired by the spin-echo 3D-FT method with 4 accumulated acquisitions. *Natto* beans were placed in a test tube 25 mm in diameter. (A) T_1-weighted images emphasised the internal structures of cotyledons (*c*) and the tissues accumulating oils (*o*) (TR 0.1 s and TE 7 ms). Vascular bundles are dots (*v*) in the cotyledons. Young roots (*r*) are observed. (B) T_2-weighted images depicting sticky materials (*s*) outside seeds (TR 1 s and TE 40 ms). (a) The 68th horizontal section in 128 slices. (b) MIP (maximum intensity projection) rendering using 67th–98th horizontal sections of the three-dimensional data. (c) The 80th vertical section in 128 slices. (d) MIP rendering using 67th–98th vertical sections of the three-dimensional data.

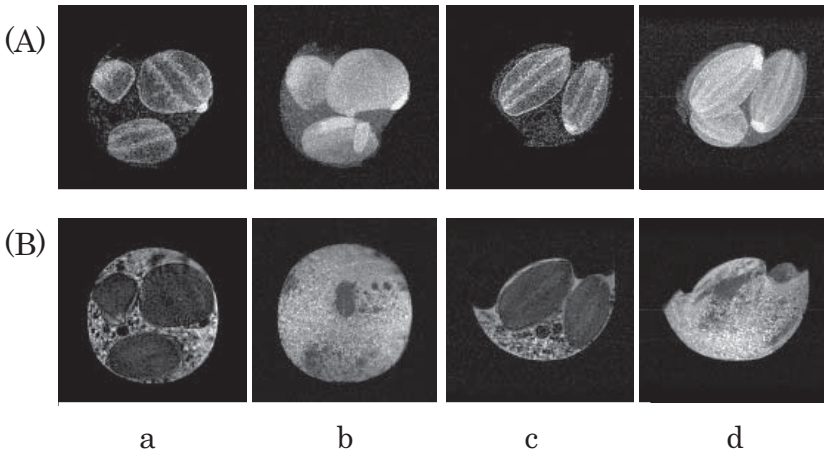

Fig. 8. Three-dimensional measurement of fermented soybeans, *natto*, after stirring. The images were acquired by the spin-echo 3D-FT method with 4 accumulated acquisitions. *Natto* beans were stirred then placed in a test tube 25 mm in diameter. (A) T_1-weighted images depicting seeds floating from the bottom of the test tube by suppressing the signals from stringy solution (TR 0.1 s and TE 7 ms). (B) T_2-weighted images with emphasised networks of stringy solution between the seeds (TR 1 s and TE 40 ms). (a) The 72nd horizontal section in 128 slices. (b) MIP rendering using 67th–98th horizontal sections of the three-dimensional data. (c) The 81st vertical section in 128 slices. (d) MIP rendering using 67th–98th vertical sections of the three-dimensional data.

and swollen 2.5-times their original size were steamed, then incubated in a warm chamber (approximately 40°C) under aerobic conditions for approximately 20 h after being inoculated with *Bacillus subtilis* (*natto*). The surface of soybeans becomes ruffled and covered with dark gray-brown wrinkles, and a stringy material is observed on the bean surfaces when they are stirred using sticks. This is the basic procedure for preparing *natto*. In the current investigation, the materials made by factory processes were obtained in a market.

In the T_1-weighted images of *natto* (Fig. 7A), the structures of cotyledons (*c*) such as the vascular bundle (*v*) and the areas where stored oils accumulated (*o*), were intensified. Oils were concentrated near the adaxial surface of the cotyledons (Fig. 7A, a and c). Interestingly, young swollen roots (*r*) were also intensified by the MIP rendering (Fig. 7A, b and d). The images indicate that the internal structures of the soybeans are well maintained after the fermentation in *natto*.

The sticky materials outside beans (*s*) generated by fermentation (Muramatsu *et al.*, 1997), which are made of γ-polyglutamic acid and β-2,6-fructan (levan) and are rich in free amino acid nutrients, were emphasised by T_2-weighted images (Fig. 7B, a and c). The materials did not uniformly cover the beans in the MIP images (Fig. 7B, b and d). The contact between the beans was lost and the beans seemed to float in the T_1-weighted images (Fig. 8A, a and c) by stirring *natto*, since the signals from the stringy solution were suppressed. The MIP images indicated that the stringy solution expanded and filled the cavities between the beans (Fig. 8A, b and d). While the nets sustaining the beans were fairly depicted in the T_2-weighted images (Fig. 8B, a and c) with suppressed soybean signals. The beans were buried in foam in the MIP images (Fig. 8B, b and d). The moderate digestion of soybeans maintaining oil storing tissues and the generation of large amounts of sticky materials are the sources of the characteristic textural feel and taste of *natto*; therefore, the MRI images are expected to provide useful information on *natto* quality.

Architecture of vasculature in fruits An interesting use of MIP images is drawing the vasculature in vegetables and fruits (MacFall and Johnson, 1994; Chudek and Hunter, 1997). Since vessels are apoplastic and superior in magnetic susceptibility to parenchyma cells, the vascular tissues can be distinguished from surrounding tissues as strong signals. The situation is suitable for MIP expression. The vascular system is closely related to fruit physiology, as has been shown for apples (Clark *et al.*, 1998; Koizumi *et al.*, 2006c).

The images of a sweet cherry (*Prunus avium* L.) cultivar 'Satonishiki' obtained by the 3D spin-echo method are shown in Fig. 9. Figure 9A is the sliced image at the centre of the fruit and depicts a thin outer skin or epidermal layer, flesh or mesocarp, a stone or putamen, and a seed in the centre. The epidermis and the thin layer just outside of the putamen that may be the vascular bundles connecting the seed to the peduncle showed strong signals due to low mobility water, and the seed had oils. Short lines with strong signal were recognised in the mesocarp and represented the sectioned vascular bundles. Figure 9B is the MIP image of the whole fruit (from 15th to 105th slices), and Fig. 9C is that of one-third of a fruit (from 30th to 60th slices). The MIP images depicted the network organisation of the vasculature running through the mesocarp of the fruit like a basket made of bamboo wires. The vasculature of the cherry is more complex than that of 'Fuji' apple (Clark *et al.*, 1998).

Similar images were obtained for a blueberry (*Vaccinium ashei* Reade), the rabbiteye cultivar (Fig. 10). The thin epidermal layer and seeds showed strong signals, and the discontinuous vasculature lines were observed in the mesocarp in the sectioned image (Fig. 10A). A large locule bearing seeds was characteristics of the fruit (Hills, 1998; Koizumi *et al.*, 2006c). The MIP image of the whole fruit (from 19th to 115th slices; Fig. 10B) shows the vasculature running through the mesocarp like a birdcage, and in the centre of it

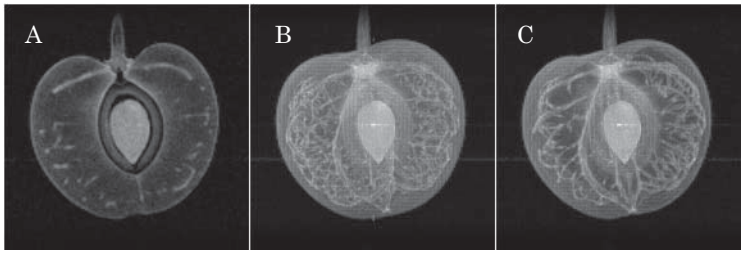

Fig. 9. Three-dimensional measurement of a sweet cherry fruit. The sweet cherry was imaged by the spin-echo 3D-FT method with TR of 0.2 s and TE of 7 ms. (A) The 60th section in 128 slices. (B) MIP expression using the whole image data of fruit (from 15th to 105th slices) showing the vasculature running through the cherry like a fine basket made of bamboo wires. (C) MIP expression using 31 sections digitally selected (from 30th to 60th slices) indicating the organisation to side direction from the seed.

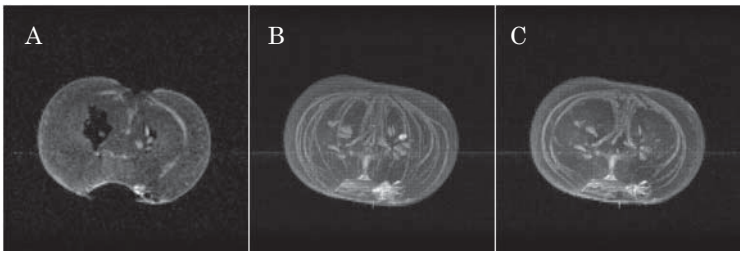

Fig. 10. Three-dimensional measurement of a blueberry fruit. The blueberry was imaged by the spin-echo 3D-FT method with TR of 0.2 s and TE of 7 ms. (A) The 62nd section in 128 slices. (B) MIP rendering using the whole image data of fruit (from 19th to 115th slices) showing vasculature running through the blueberry like a birdcage, with several seeds. (C) MIP rendering using 24 sections digitally selected (from 61st to 84th slices) simplifying the overlapping of vasculature and indicating the connection between seeds and the vascular bundle.

there are several seeds. All vascular bundles are connected at the peduncle. The MIP image of one-fourth of the fruit (from 61st to 84th slices; Fig. 10C) simplifies the overlapping of vasculature and indicates that the seeds do not connect with vascular bundles in the mesocarp but with those running through the endocarp leading to the peduncle.

Conclusions

The current paper reports a dedicated MRI apparatus for use by small numbers of researchers working in similar directions in a certain field. The apparatus is moderately specific, e.g., the resolution of the images is 117 μm with 1.8-mm slice thickness in 2D measurements and 234 μm in 3D measurements for materials 30 mm in diameter. Time-lapse images could trace the thawing processes of frozen food materials (Figs. 2, 4 and 5), and three-dimensional imaging provided a clear morphology of meats (Fig. 3), fermented soybeans (Figs. 7 and 8) and fruits (Figs. 9 and 10). The relaxation time-weighted images distinguished and differently depicted the distribution between the fat and the muscle tissues of meat foods (Fig. 3), and between the oil accumulating tissues in soybeans and sticky materials generated by fermentation outside the beans (Figs. 7 and 8). The volume rendering using three-dimensional data demonstrated the spatial disposition of the fat tissue in pork (Fig. 3), and the MIP rendering drew soft networks of the stringy solution on the outside of *natto* beans (Fig. 8), and the fine vascular systems in fruits (Figs. 9 and 10). These images were acquired with adequate clarity and spatial resolution by a small, lightly equipped MRI apparatus devised in the current investigation. The machine is easy to operate and relatively free from complicated maintenance. Its construction cost was less than one-fifth that of usual microMRI apparatuses. The small size and the orientation for personal use are trends in modern science and technology similar to notebook computers or hand-held telephones. Easy operation and low-maintenance are other trends in modern society. In this context, we are convinced that small dedicated MRI is useful for the developmental research and quality evaluation of food materials and agricultural products, and also for exploring new applications of MRI in food science and agriculture.

Acknowledgements We wish to thank Neomax Co., Ltd. for its assistance in devising a fine stabiliser for controlling the temperature of the permanent magnet. We thank the Ministry of Agriculture, Forestry and Fisheries for their support in constructing a small MRI through the Technical Development Program for "Making agribusiness in the form of utilising concentrated know-how from private sector" and the Society for Techno-innovation of Agriculture, Forestry and Fisheries for managing the project. We are also grateful to the two anonymous referees of *Food Science and Technology Research* for their substantial and valuable advice. Part of this work was supported by KAKENHI (No.19500672) from the Ministry of Education, Culture, Sports, Science and Technology.

References

Beauvallet, C. and Renou, J.P. (1992). Applications of NMR spectroscopy in meat research. *Trends Food Sci. Technol.*, **3**, 241-246.

Brennan, R.M., Chudek, J.A., Goodman, B.A., Simpson, E.J. and Hunter, G. (1997). Non-destructive visualisation in three dimensions of freezing events in flowers of blackcurrant (*Ribes nigrum* L.) using spin-echo NMR microscopy. *Magn. Reson. Imaging*, **15**, 1085-1090.

Chudek, J.A. and Hunter, G. (1997). Magnetic resonance imaging of plants. *Prog. Nucl. Magn. Reson. Spectrosc.*, **31**, 43-62.

Clark, C.J., MacFall, J.S. and Bieleski, R.L. (1998). Loss of watercore from 'Fuji' apple observed by magnetic resonance imaging. *Sci. Hortic.*, **73**, 213-227.

Constantinesco, A., Choquet, P., Cauffet, G., Fournier, J.M., Ravier, S., Drillon, J.M. and Aubert, G. (1997). Low-field dedicated and desktop magnetic resonance imaging systems for agricultural and food applications. *Magn. Reson. Chem.*, **35**, S69-S75.

Faust, M., Wang, P.C. and Maas, J. (1997). The use of magnetic resonance imaging in plant science. *Hortic. Rev.*, **20**, 225-266.

Guiheneuf, T.M., Parker, A.D., Tessier, J.J. and Hall, L.D. (1997). Authentication of the effect of freezing/thawing of pork by quantitative magnetic resonance imaging. *Magn. Reson. Chem.*, **35**, S112-S118.

Haishi, T., Uematsu, T., Matsuda, Y. and Kose, K. (2001). Development of a 1.0 T MR microscope using a Nd-Fe-B permanent magnet. *Magn. Reson. Imaging*, **19**, 875-880.

Hall, L.D., Evans, S.D. and Nott, K.P. (1998). Measurement of textural changes of food by MRI relaxometry. *Magn. Reson. Imaging*, **16**, 485-492.

Hills, B. (1998). "Magnetic Resonance Imaging in Food Science." John Wiley & Sons, New York.

Kerr, W.L., Kauten, R.J., McCarthy, M.J. and Reid, D.S. (1998). Monitoring the formation of ice during food freezing by magnetic resonance imaging. *Lebensm.-Wiss. u.- Technol.*, **31**, 215-220.

Koizumi, M., Naito, S., Haishi, T., Utsuzawa, S., Ishida, N. and Kano, H. (2006a). Thawing of frozen vegetables observed by a small dedicated MRI for food research. *Magn. Reson. Imaging*, **24**, 1111-1119.

Koizumi, M., Naito, S., Kano, H., Ishida, N. and Haishi, T. (2006b). Fermented soybeans, *natto*, observed by a compact MRI. *The Food Industry*, **49**, 57-71 (in Japanese).

Koizumi, M., Kano, H., Naito, S., Ishida, N. and Tanaka, K. (2006c). MRI researches in the preservation of fruits. *Nippon Shokuhin Kagaku Kogaku Kaishi*, **53**, 237-247 (in Japanese).

Laurent, W., Bonny, J.M. and Renou, J.P. (2000). Muscle characterisation by NMR imaging and spectroscopic techniques. *Food Chem.*, **69**, 419-426.

MacFall, J.S. and Johnson, G.A. (1994). The architecture of plant vasculature and transport as seen with magnetic resonance microscopy. *Can. J. Bot.*, **72**, 1561-1573.

McCarthy, M.J. (1994). "Magnetic Resonance Imaging in Foods." Chapman & Hall, New York.

Muramatsu, K., Nagai, T., Sato, S., Ochiai, Y., Ishimura, N., Ito, Y. and Kiuchi, K. (1997). Stimulative effect of phytone on the production of sticky materials in *Bacillus subtilis* (*natto*). *Nippon Shokuhin Kagaku Kogaku Kaishi*, **44**, 812-815 (in Japanese).

Price, W.S., Ide, H., Ishikawa, M. and Arata, Y. (1997). Intensity changes in ^{1}H-NMR micro-images of plant materials exposed to subfreezing temperatures. *Bioimages*, **5**, 91-99.

Renou, J.P., Foucat, L. and Bonny, J.M. (2003). Magnetic resonance imaging studies of water interactions in meat. *Food Chem.*, **82**, 35-39.